



TITLE:

Tin-Doped Inorganic Amorphous Films for Use as Transparent Monolithic Phosphors.

AUTHOR(S):

Masai, Hirokazu; Miyata, Hiroki; Yamada, Yasuhiro; Okumura, Shun; Yanagida, Takayuki; Kanemitsu, Yoshihiko

CITATION:

Masai, Hirokazu ...[et al]. Tin-Doped Inorganic Amorphous Films for Use as Transparent Monolithic Phosphors.. Scientific reports 2015, 5: 11224.

ISSUE DATE:

2015-06-10

URL:

<http://hdl.handle.net/2433/201625>

RIGHT:

This work is licensed under a Creative Commons Attribution 4.0 International License. The images or other third party material in this article are included in the article's Creative Commons license, unless indicated otherwise in the credit line; if the material is not included under the Creative Commons license, users will need to obtain permission from the license holder to reproduce the material. To view a copy of this license, visit <http://creativecommons.org/licenses/by/4.0/>

SCIENTIFIC REPORTS

OPEN

Tin-Doped Inorganic Amorphous Films for Use as Transparent Monolithic Phosphors

Hirokazu Masai¹, Hiroki Miyata¹, Yasuhiro Yamada^{1,*}, Shun Okumura¹, Takayuki Yanagida^{2,**} & Yoshihiko Kanemitsu¹

Received: 16 February 2015

Accepted: 19 May 2015

Published: 10 June 2015

Although inorganic crystalline phosphors can exhibit high quantum efficiency, their use in phosphor films has been limited by a reliance on organic binders that have poor durability when exposed to high-power and/or high excitation energy light sources. To address this problem, Sn^{2+} -doped transparent phosphate films measuring several micrometers in thickness have been successfully prepared through heat treatment and a subsequent single dip-coating process. The resulting monolithic inorganic amorphous film exhibited an internal quantum efficiency of over 60% and can potentially utilize transmitted light. Analysis of the film's emissivity revealed that its color can be tuned by changing the amount of Mn and Sn added to influence the energy transfer from Sn^{2+} to Mn^{2+} . It is therefore concluded that amorphous films containing such emission centers can provide a novel and viable alternative to conventional amorphous films containing crystalline phosphors in light-emitting devices.

Recent advances in light-emitting diodes (LEDs) have been accompanied by the development of new phosphors^{1–5} for light-emitting devices^{6–11} the luminescence of which depends on the emission center used and its surrounding matrix. At present, virtually all practical light-induced emission devices are predominantly fabricated from a mixture of powdered phosphors and organic binders^{12–14}; however, the damage caused to organic binders such as silicone resins by high-power and/or high-energy excitation light sources (e.g., high power LEDs) tends to reduce their service life. Furthermore, light scattering at the interface between the powdered phosphors and the surrounding matrix is not inherently eliminated in conventional devices that consist of a crystalline phosphor and binder. Consequently, transparent inorganic films capable of light-wave conversion will likely be required for white LED or sunlight converter applications in the near future. In particular, monolithic inorganic (and ideally amorphous) materials possessing good emissivity will be required for industrial applications of large-area devices.

A solution to this lies in the preparation of monolithic, inorganic bulk-glass phosphors containing an emission center. Since such a structure has no grain boundaries between the emission center and surrounding glass, the loss of external efficiency is expected to be greatly reduced. Investigation into the emission properties of amorphous glasses has so far been mainly limited to rare earth (RE)-containing glasses^{15–19} whose emission is almost independent of the coordination state compared to other emission centers; however, uncertainty as to the future stability of RE supplies has seen RE-free materials extensively examined in other fields. Thus, it would appear that a monolithic RE-free material possessing good emission properties is what will be required for future applications.

If we consider the transition probability of emission centers then a parity-allowed transition is favorable to attaining high emission intensity. For instance, a non-RE ns^2 -type emission center ($n \geq 4$)

¹Institute for Chemical Research, Kyoto University, Gokasho, Uji, Kyoto 611-0011, Japan. ²Kyushu Institute of Technology, 2-4 Hibikino, Wakamatsu-ku, Kitakyushu 808-0196, Japan. *Current address: Graduate School of Science, Chiba University, 1-33 Yayoi, Inage, Chiba 263-8522, Japan. **Current address: Graduate School of Materials Science, Nara Institute of Science and Technology, 8916-5 Takayama-Cho, Ikoma, Nara 630-0192, Japan. Correspondence and requests for materials should be addressed to H.M. (email: masai_h@scl.kyoto-u.ac.jp)

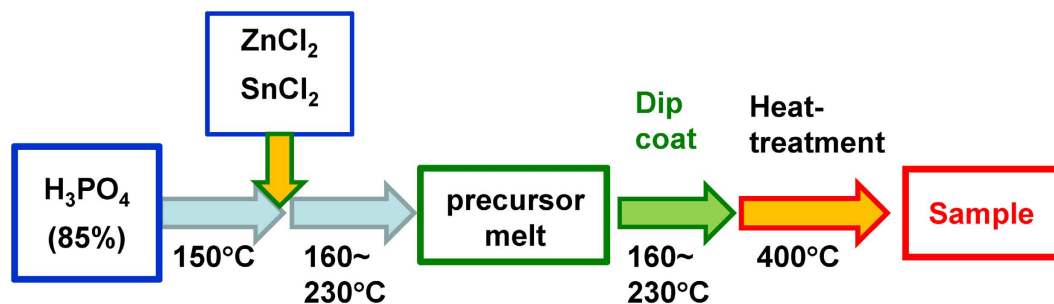


Figure 1. Preparation method for a SnO-ZnO-P₂O₅ film.

possessing ns^2 - $nsnp$ transition^{20–27} has a sufficiently high transition probability for use a practical phosphor, as is seen with Sb^{3+} - or Mn^{2+} -doped calcium halophosphate²⁷. Our group has therefore focused on ns^2 -type cations, and has previously reported blue light emission from Sn^{2+} -doped ZnO-P₂O₅ glass^{28,29}. Various light emissions have also been reported from a MnO-doped SnO-ZnO-P₂O₅ glass^{30,31}, including an intense UV-excited emission comparable to that of a crystal phosphor such as MgWO₄. Of particular note was the finding that a transparent RE-free bulk oxide glass attains high quantum efficiency, suggesting that despite being typically thought of as *passive* materials with regards to light, they may in fact have great potential for *active* light conversion^{28–32}. Although the use of bulk glass presents one solution to providing a suitable light conversion technique, it is poorly suited to applications in which it is desirable to utilize established techniques for the fabrication of light-emitting devices such as white LEDs or solar cells. Consequently, there is a need to develop methods for preparing thin-film phosphors that can be readily adapted to large-area devices.

Broad emission from a Sn^{2+} center in a SnO-ZnO-P₂O₅ amorphous thin film under excitation with UV light has been recently reported³³ with this film being produced from a precursor solution of SnCl₂, ZnCl₂, 85% H₃PO₄, and ethanol by dip-coating and heat-treatment. When compared with conventional sol-gel techniques, this method yields a much greater film density and a thickness of several microns; however, both the flatness and transparency of the film were insufficient due to the evaporation of the solvent or water. Thus, in order to improve the film condition, we have since focused on a solvent-free acid-base reaction that was previously used for the preparation of organic-inorganic hybrids³⁴. In this technique, a spontaneous reaction between Si-Cl and P-OH forms a Si-O-P network through the elimination of HCl, which suppresses foaming and produces a remarkable volume shrinkage during heat treatment. It is expected that transparent inorganic amorphous films possessing photoluminescent (PL) properties can be obtained using this solvent-free technique, and in this study is used to prepare Sn^{2+} -containing oxide phosphor films. By studying the luminescence properties of these films, this report provides a valuable benchmark for transparent and highly photoluminescent inorganic films produced using an industrially viable fabrication technique.

Results

Preparation and examination of emission properties. The transparent film formation region of the SnO-ZnO-P₂O₅ ternary film system was first investigated according to the preparation scheme shown in Fig. 1, while the film system itself shown in Fig. 2 along with the bulk glass formation region reported by Morena³⁵. This solvent-free preparation technique resulted in a composition that is at least 40 mol% P₂O₅, but the region in which this amorphous film is formed differs notably from that of bulk glass prepared using conventional melt-quenching methods³⁵. Indeed, several samples were observed to turn opaque following heat treatment, which was attributed to the crystallization of zinc phosphate phases such as Zn₂P₂O₇. Figure 3 shows the ³¹P Nuclear Magnetic Resonance (NMR) spectra of a 10SnO-40ZnO-50P₂O₅ precursor melt and an amorphous film produced from it by heat-treatment, the former consisting of Q⁰ units (Fig. 3(a)) prior to chloride addition that are also clearly observed in the precursor melt prior to dip coating (Fig. 3(b)). The generation of phosphate chain Q² units (Fig. 3(c)) during heat treatment is therefore confirmed; but since it is often reported that phosphate units result in low water durability, whichever chemical composition produces the least amount of P₂O₅ is clearly the most favorable. Thus, in order to examine the relationship between the chemical composition and PL properties, we selected the $xSnO$ -(50- x)ZnO-50P₂O₅ (mol%) system and prepared transparent films with various SnO:ZnO molar ratios. Table 1 shows the chemical composition of SnO-ZnO-P₂O₅ films obtained by energy dispersive X-ray (EDX)-Scanning Electron Microscope (SEM) measurement, which confirmed that there is only a small difference between the nominal and actual composition.

Most of the amorphous films produced were found to be colorless and transparent both by visual observation (Fig. 4a) and from their optical absorption spectra (Fig. 4b, and supplemental figure 1). Since conventional deposition techniques for inorganic films such as dip- or spin-coating produce films with a submicron scale thickness, even with the addition of a thickener, such techniques are difficult to

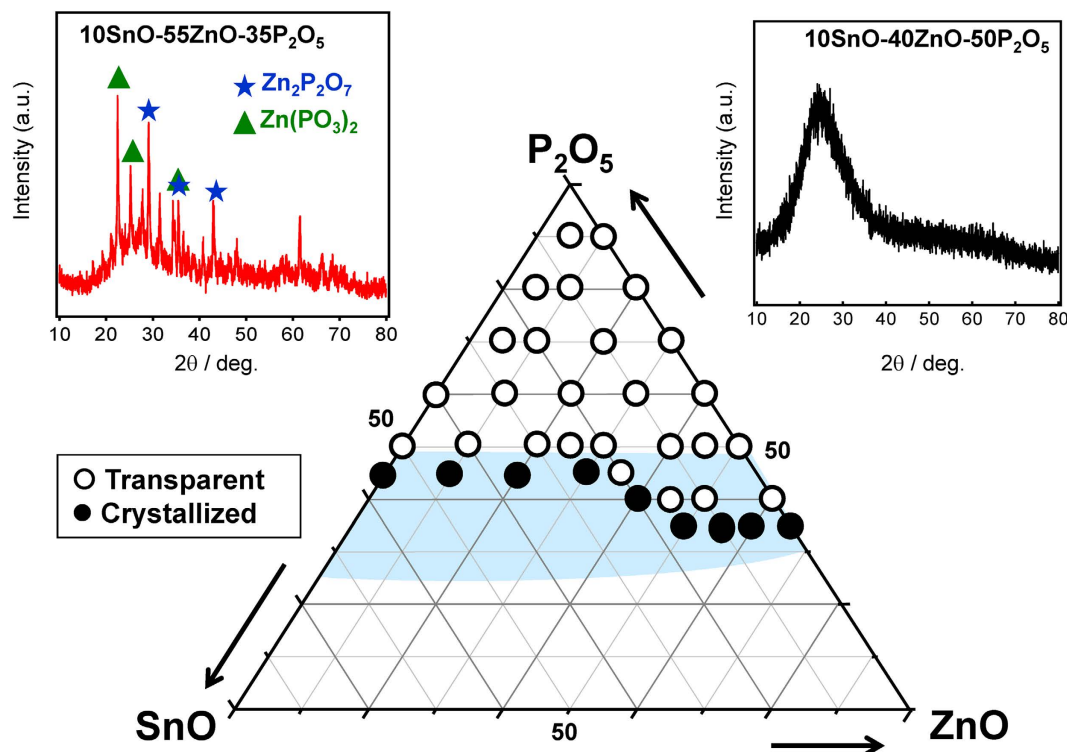


Figure 2. SnO-ZnO-P₂O₅ ternary amorphous film system, together with the bulk glass formation region reported by Morena³⁵. The open and closed circles indicate amorphous and crystallized films, as shown in the typical XRD patterns.

adapt to producing micron-thick films suitable for photon energy conversion. Moreover, conventional procedures inherently require coating or heat-treatment cycles to obtain a thick film, whereas we have confirmed that a slower elevation rate is all that is needed to achieve film thickness in the order of several micrometers. Indeed, the viscous nature of the precursor melt used in this study allows films several microns in thickness to be obtained by using just one dip-coating and heat-treatment procedure (*i.e.* a single dip-heat-treatment process). The TEM and SEM images are shown in supplemental fig. 2. From these images, it is found that the amorphous thick film without crystallites or cracks was successfully obtained. Figure 4c shows the surface profile of the 10SnO-40ZnO-50P₂O₅ film at different points, with the upper part of the film exhibiting a thickness of about 10 μ m (elevation rate: 1 mm/s) and a relatively smooth surface ($R_a \sim 0.1 \mu$ m). The roughness ($R_a \sim 1 \sim 2 \mu$ m) was, however, also observed in the lower part of the film due mainly to the increase in film thickness during the dip-coating process. Furthermore, the transparent film exhibited a clear blue-light emission under irradiation by UV light, whereas no PL properties were observed in the case of a Sn-free sample. Thus, it is important to emphasize that the present coating method is quite different from existing techniques in that it can achieve micron-thick films with a single process that is suitable for industrial application.

Because Sn²⁺ is a metastable species, and therefore easily affected by the preparation conditions^{36,37} it is important to examine the valence state of Sn in the matrix. Figure 5 shows Sn K-edge XANES spectra of several x SnO-(50- x)ZnO-50P₂O₅ films ($x = 5$ and 10), with the spectra for SnO and SnO₂ also provided for reference. If we take the absorption edge energy, E_0 , to be the energy at the zero-intercept of the second derivative, we can evaluate the oxidation state of the Sn cation from the E_0 value; $|\Delta(E_0(\text{SnO}) - E_0(\text{film}))|$ being calculated as less than 1.7 eV in all instances. Considering the resolution of the measurement ($\Delta E/E \sim 6 \times 10^{-5}$; ~ 1.75 eV), it is assumed that the difference between values is insignificant. Thus, the Sn K-edge XANES spectra suggest that the percentage of Sn²⁺ to total Sn in x SnO-(50- x)ZnO-50P₂O₅ films is nearly 100%. This is consistent with results in the literature that suggest that a valence change of Sn²⁺ to Sn⁴⁺ occurs at temperatures over 650 °C in air³⁸.

Figure 6 shows PL-PLE spectra of x SnO-(50- x)ZnO-50P₂O₅ films with different SnO contents. In order to better understand the spectral change the intensities were normalized using the maximum value recorded, which was observed in the 10SnO-40ZnO-50P₂O₅ film. The PLE spectra were measured at the peak photon energy of each PL spectrum. The PL spectra show little dependence on the SnO concentration, but the excitation peak energy does slightly red-shift with increasing SnO concentration. Because the Sn²⁺ emission center possesses electrons in the outermost shell, its emission spectrum is strongly affected by the coordination field^{20,36,39}. The unchanged emission spectra of Sn²⁺ therefore indicate that

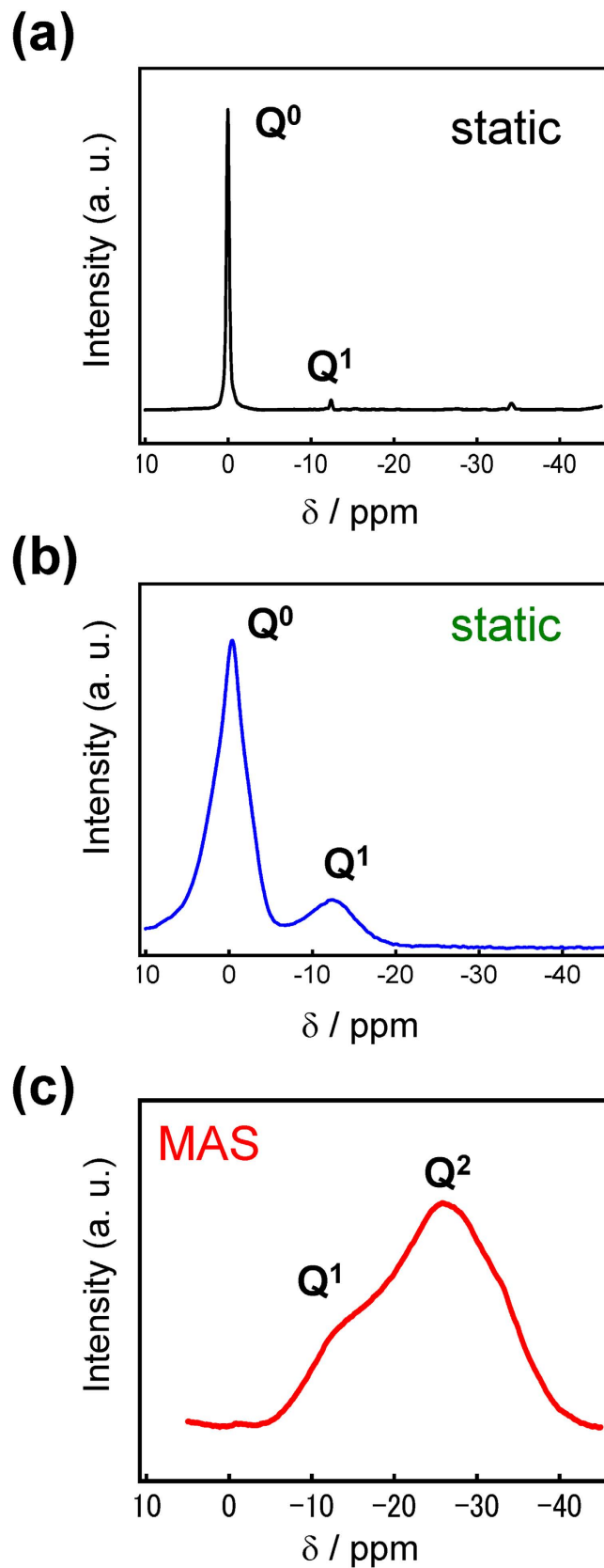


Figure 3. ^{31}P NMR spectra of a 10SnO-40ZnO-50P₂O₅ precursor melt and amorphous film after heat-treatment. (a) Precursor melt prior to addition of chlorides. (b) Precursor melt prior to dip coating. (c) Amorphous film.

Nominal Chemical composition/mol%	Molar ratio measured by EDX SEM/mol%		
	SnO (± 1)	ZnO (± 2)	P ₂ O ₅ (± 2)
5SnO-45ZnO-50P ₂ O ₅	5	41	54
10SnO-40ZnO-50P ₂ O ₅	8	38	54
15SnO-35ZnO-50P ₂ O ₅	13	34	53

Table 1. Chemical composition of SnO-ZnO-P₂O₅ films obtained by EDX-SEM measurement.

the local coordination states of the Sn²⁺ center are not so diverse, even though the host matrix is amorphous. Figure 7 shows a streak image of a 10SnO-40ZnO-50P₂O₅ film obtained by excitation at 250 nm, revealing that the timescale of film decay is in the order of microseconds and that it can be classified as a triplet-singlet relaxation of the Sn²⁺ center. The decay constant $\tau_{1/e}$ of the main band is about 8 μ s, which is longer than that previously reported for bulk glasses^{29,32}. Since this decay constant depends on the concentration, the observation that it remains the same suggests that the actual concentration in the Sn²⁺ center is below 1 mol%²⁹. It is also notable that the emission peak energy does not shift to lower energies with increasing time, as was the case with Sn²⁺-doped zinc oxide glass phosphors^{29,32}. Although the local environment in glass materials can be estimated from the emission lifetime^{40,41}, it is hard to determine some specific sites from the decay of the film. Therefore, we assume that Sn²⁺ emission centers exist with Gaussian distribution. On the basis of this emission spectra and streak image we believe that not all of the Sn²⁺ centers are good emitters/absorbers in the film, despite it containing 10 mol% SnO. In other words, only a limited number of the Sn²⁺ ions are capable of functioning as emission centers for PL. If the distribution of Sn²⁺ in bulk glass prepared by melt-quenching is also taken into consideration then the film can be expected to possess heterogeneity to at least a nanometer scale (phase-separated structure), which would explain why the concentration at which the fluorescence is quenched is around 10 mol% SnO. In other words, if we can control the local coordination state of the Sn²⁺ centers, then the chemical composition of the film can be drastically varied. Figure 8 shows the correlation between internal quantum yield (QY) and the amount of SnO in xSnO-(50-x)ZnO-50P₂O₅ films, revealing the QY of these films to be almost constant (over 60%) below 10 mol% SnO, but to decrease with increasing SnO content. This contrasts with previous reports on bulk glass phosphors^{28-33,36} in which more than a 20% decrease of QY is observed. As mentioned above, it is expected that some Sn²⁺ species do not function as an emission center, and so considering the relationship between the concentration of Sn²⁺ and the QY value, it is suggested that several Sn²⁺ species cluster to decrease the QY value. On the other hand, from the optical absorption spectrum, there is evidently sufficient excitation light absorbed by a film with a thickness of about 10 μ m to ensure blue light emission.

Demonstration of white light emission. Figure 9a shows normalized PL spectra of γ MnO-10SnO-40ZnO-50P₂O₅ films (where $\gamma = 0, 0.1, 0.5, 1, 2$, and 5), while the inset shows photographs of several films ($\gamma = 0, 1$, and 5) under 254 nm UV irradiation. These PLE spectra are shown in supplemental figure 3. Note that the color coordination positions continuously change from blue to red with the addition of MnO, and that these emission spectra consist of two broad bands attributable to the Sn²⁺ and Mn²⁺ centers that have also been observed in other materials^{30,42}. Peak deconvolution using Gaussian function revealed that these two peaks show little change in their emission band or half-width, indicating that the local coordination of Sn²⁺ and Mn²⁺ is hardly affected by the MnO concentration. Moreover, the emission intensity of SnO is reduced when the amount of MnO is increased, suggesting that energy is transferred between them. In order to confirm this energy transfer emission decay curves of MnO-free and MnO-doped ($\gamma = 1.0$, and 5.0) 10SnO-40ZnO-50P₂O₅ films were obtained, as shown in Fig. 9b, with the decay values being calculated from an integral of the photon number in the streak image within the 2.53–2.70 eV region. With the addition of MnO, the decay constant of the Sn²⁺ center with Mn²⁺ cations ($\tau_{1/e}$) is reduced, indicating that an energy transfer from Sn²⁺ to Mn²⁺ does occur. The energy transfer efficiency (η_{ET}) is calculated from the $\tau_{1/e}$ values using the formula⁴³:

$$\eta_{ET} = 1 - \tau_{1/e} / \tau_{1/eD} \quad (1)$$

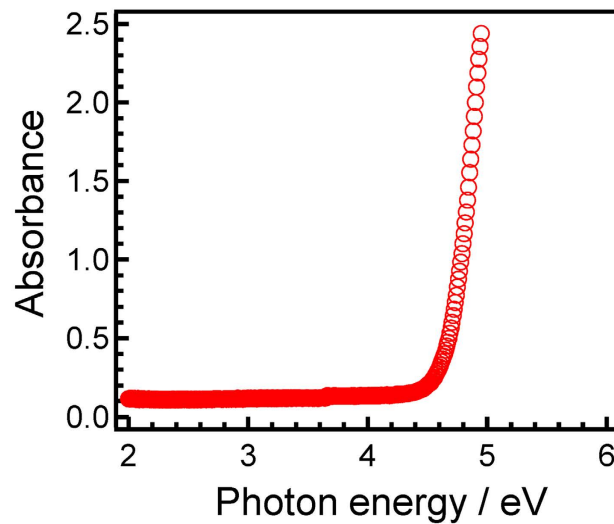
where $\tau_{1/eD}$ is the decay constant of a Sn²⁺ center without a Mn²⁺ cation. Using Equation (1), the η_{ET} values of the 1MnO-doped and 5MnO-doped 10SnO-40ZnO-50P₂O₅ films were found to be 21 and 88%, respectively (see inset of Fig. 9b). As these η_{ET} values are roughly dependent on the MnO concentration, the present data shows no evidence of the local Sn²⁺-Mn²⁺ clustering structure that has been previously suggested to form in alkali halide^{42,44}.

Figure 10 shows the correlation between QY and the amount of MnO in γ MnO-10SnO-40ZnO-50P₂O₅ films. The QY values of the MnO-doped films ($\gamma \leq 2$) were all over 60%; which, in combination with the similarity of their blue-white-red light emission to that of bulk glass, confirms their potential application as a transparent phosphor for large-area devices. Furthermore, it is possible to

(a)



(b)



(c)

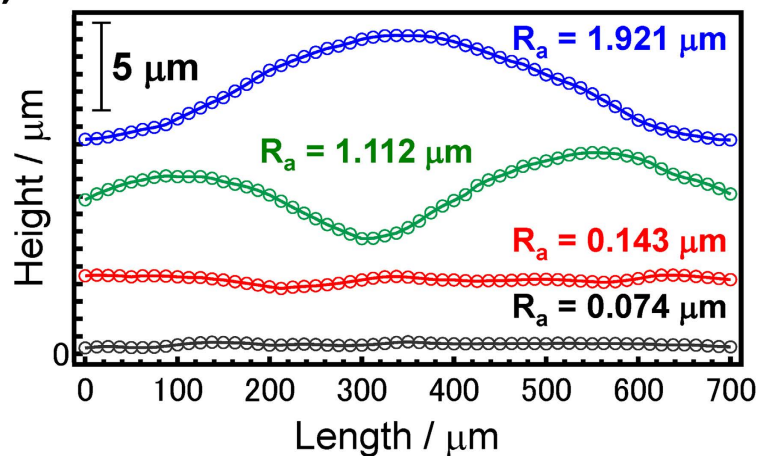


Figure 4. Optical properties of a SnO-ZnO-P₂O₅ amorphous film. (a) Photograph of a 10SnO-40ZnO-50P₂O₅ film with and without UV irradiation (4.88 eV). The clearly visible blue light emission is due to the Sn²⁺ center. (b) Optical absorption spectrum for a 10SnO-40ZnO-50P₂O₅ film 10 μm in thickness. (c) Surface profiles of the 10SnO-40ZnO-50P₂O₅ film at different measurement points.

add other elements to these films to better control their emissivity (such as using metal halides like lanthanide-chloride to control the color) or to improve their mechanical and/or thermal properties.

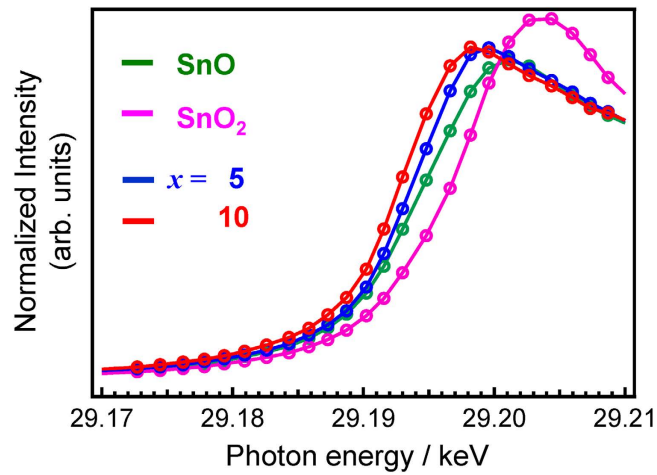


Figure 5. Sn K-edge XANES spectra of $x\text{SnO}-(50-x)\text{ZnO}-50\text{P}_2\text{O}_5$ films ($x=5$ and 10). Also shown for comparison are the spectra for SnO and SnO_2 .

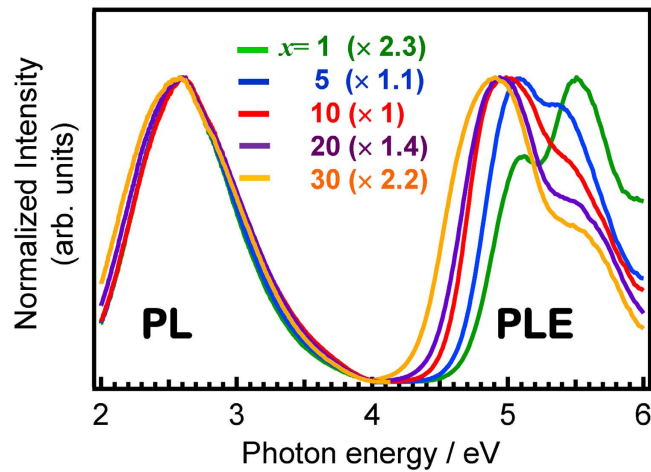


Figure 6. Normalized PL-PLE spectra of $x\text{SnO}-(50-x)\text{ZnO}-50\text{P}_2\text{O}_5$ films.

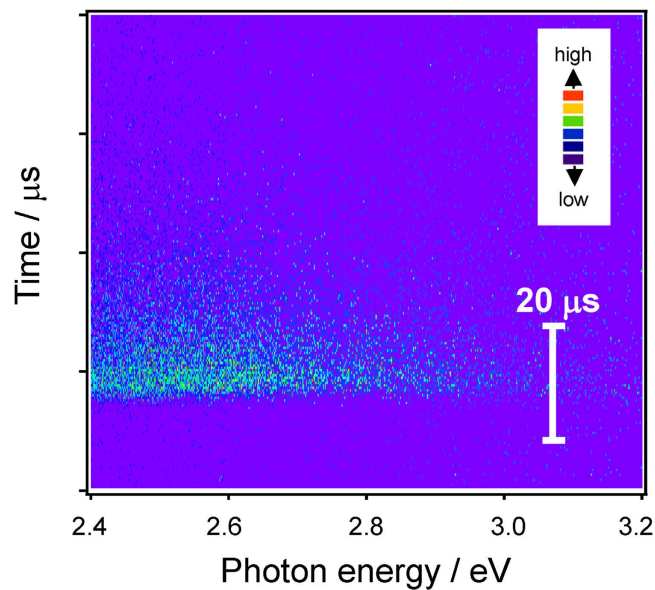


Figure 7. Streak image of a $10\text{SnO}-40\text{ZnO}-50\text{P}_2\text{O}_5$ film obtained by excitation at 250 nm .

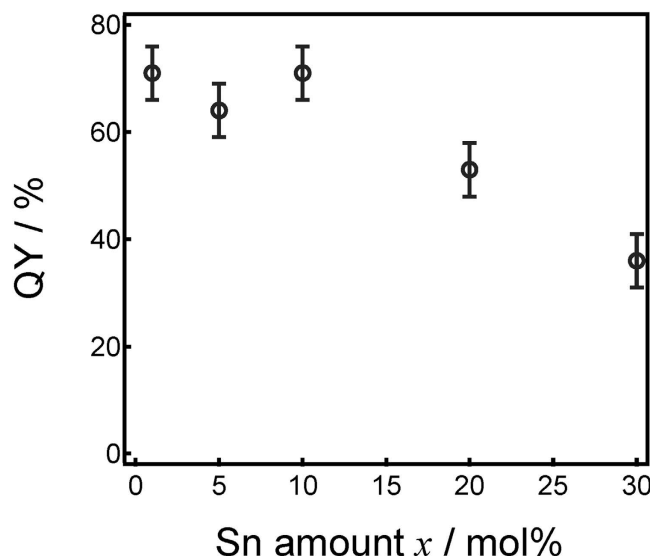


Figure 8. Correlation between internal quantum efficiency (QY) and the amount of SnO in $x\text{SnO}-(50-x)\text{ZnO}-50\text{P}_2\text{O}_5$ films.

In particular, the recent development of a deep-UV LED^{7–10} suggests a very clear possibility for novel film-type emission devices in the near future.

Discussion

In the present study, we have demonstrated the UV-excited light emission of Sn^{2+} -doped zinc phosphate films produced from a precursor melt by a solvent-free acid-base reaction. We have confirmed that the film can be also prepared on commercially available borosilicate or soda lime silicate (slide glass) plates. Importantly, this fabrication method allows inorganic films with a thickness on the order of several microns to be produced in a single dip-coating process. One of the main reasons for thick film is the high viscosity of the precursor melt containing no solvent. High-viscous precursor melt, whose viscosity depends on the temperature, make it possible to prepare thickness film without crack. This allows the transparent phosphor to utilise the energy of both converted and transmitted light. The presence of both phosphor crystals (micrometre size) and nanocrystallites also means that these monolithic films can reduce the optical loss of transmitted light produced by luminescence. Moreover, although their chemical durability is still insufficient for direct practical use owing to hygroscopicity, this could be potentially overcome by chemical or physical means such as a luminous layer in an organic LED (OLED).

The Sn^{2+} contained within the film exhibits an effective T_1-S_0 relaxation, this being despite the presence of nanoscale heterogeneity. Recently, we reported that the emission of the Sn^{2+} center does not reflect the average (macroscopic) basicity of the glass, but instead reflects the local basicity of the emission center⁴⁵. This indicates that the macroscopic randomness and composition are not critical factors for attaining a high quantum efficiency, and that amorphous materials can exhibit high conversion efficiencies comparable to those of crystalline phosphors if the microscopic local coordination states of the emission centers are controlled. However, as pointed out earlier, not all Sn^{2+} species are a good emission center. Thus, although the local coordination state of a Sn^{2+} center needed to attain the highest light conversion has not yet been clarified, monolithic inorganic phosphor films exhibiting good emissivity can nevertheless be obtained by tailoring the local coordination state of the emission center. Therefore, the amorphous film exhibiting the internal quantum efficiency of over 60% can be improved from viewpoint of energy conversion. Moreover, its emission color can be fine-tuned by altering the energy transfer from Sn^{2+} to acceptors, such as Mn^{2+} . These results confirm the validity of this approach, which is of great significance to the fabrication of transparent films exhibiting various light-wave shifts.

Methods

Preparation of SnO-doped zinc phosphate films. The starting materials for the $\text{SnO}-\text{ZnO}-\text{P}_2\text{O}_5$ film were SnCl_2 , ZnCl_2 , and 85% H_3PO_4 . The film was prepared by conventional dip-coating at 160–230 °C using a precursor melt prepared by first heating 85% H_3PO_4 in a glass beaker to 120–150 °C for 3 h to remove any water or residual OH groups, after which SnCl_2 and ZnCl_2 were added at the same temperature. Next, the melt was gradually heated to 160–230 °C for 1 h under constant stirring in the ambient atmosphere to obtain a transparent homogeneous precursor melt. In the case of the Mn^{2+} -co-doped samples, MnCl_2 was added simultaneously with the SnCl_2 and ZnCl_2 . In either case, a thin film of the melt was produced by dip-coating a pure SiO_2 glass substrate at an elevation rate of 0.1 mm/s.

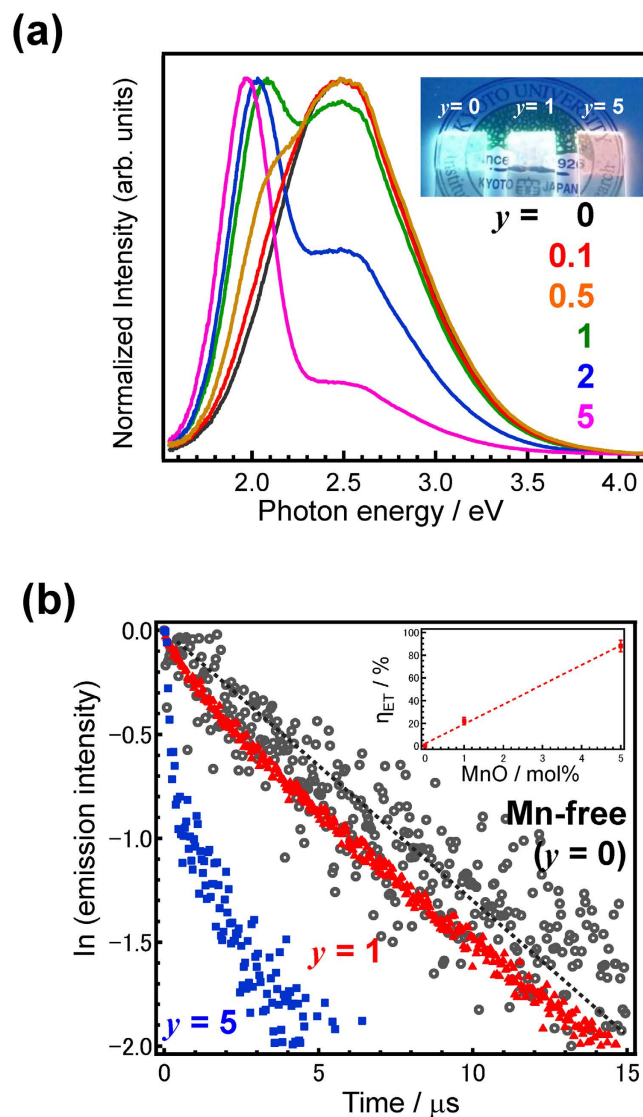


Figure 9. Emissive properties of a $y\text{MnO}-10\text{SnO}-40\text{ZnO}-50\text{P}_2\text{O}_5$ amorphous film. (a) Normalized PL spectra of a $y\text{MnO}-10\text{SnO}-40\text{ZnO}-50\text{P}_2\text{O}_5$ film excited at 4.96 eV. The inset shows a photograph of several films ($y = 0, 1$, and 5) under UV irradiation at 254 nm. (b) Emission decay curves of $y\text{MnO}-10\text{SnO}-40\text{ZnO}-50\text{P}_2\text{O}_5$ ($y = 0, 1$, and 5) films, as calculated from the integral of the photon number in the streak image within the 2.53–2.70 eV region. Inset shows the η_{ET} values as a function of MnO amount.

Afterward, the sample was placed in an electric furnace under the ambient atmosphere at 400 °C for 10 min to obtain the final film.

Analysis methods. The surface profile of the film was measured using a Surfcomer SE-30D (Kosaka Laboratory). Energy dispersive X-ray-SEM measurement was performed using a JSM-6500F microscope (JEOL). The ^{31}P NMR spectra were measured using a CMX-400 NMR spectrometer (JEOL) at a frequency of 161.80 MHz, and the chemical shifts were estimated with respect to H_3PO_4 in a D_2O solution (0 ppm). The ^{31}P magic angle spinning (MAS) NMR spectrum was measured at a spin rate of 10 kHz and a pulse delay of 5 s, and a fine powder produced by pulverising the dip-coated glass was used for measurement in the case of the thin films. The PL and PLE spectra were measured at room temperature using an F-7000 fluorescence spectrophotometer (Hitachi) with appropriate band pass filters for the excitation (5 nm) and the emission (3 nm) required for PL measurements. The absorption spectra were measured from the centres of the films using a U3500 UV-vis-NIR spectrophotometer (Hitachi). The chemical composition of the films was determined by EDX-SEM measurement for a 500 nm spot size using a JSM-6500F (JEOL). Furthermore, XRD measurements were made to ascertain the crystallization behaviour of the film using a RINT2100 instrument (Rigaku). The emission decay at room temperature was evaluated using a streak camera in conjunction with a monochromator. The light source used for photoexcitation

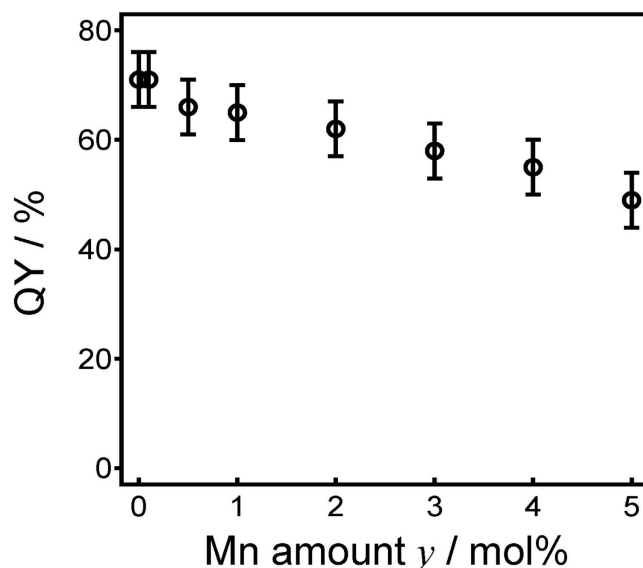


Figure 10. Correlation between QY and the amount of MnO in $y\text{MnO}-10\text{SnO}-40\text{ZnO}-50\text{P}_2\text{O}_5$ films.

was an optical parametric amplifier system based on a regenerative amplified mode-locked Ti:sapphire laser (Spectra Physics) with a pulse duration of 150 fs and a repetition rate of 1 kHz. The photon energy was 4.96 eV, which corresponded to the peak energy of the PLE spectra. The Sn K-edge (29.3 keV) XAFS spectra were measured at BL01B1 of SPring-8 (Hyogo, Japan) using a Si (311) double crystal monochromator in the transmission mode (Quick Scan method) at room temperature. The storage ring was operated at an energy of 8 GeV with a typical current of 100 mA. The internal quantum efficiency was measured using a Quantaaurus-QY (Hamamatsu Photonics), which possesses an integrating sphere in order to measure absolute efficiency. The errors of the measurement were $\pm 3\%$.

References

- Blasse, G. & Bril, A. Investigation of some Ce^{3+} -activated phosphors. *J. Chem. Phys.* **47**, 5139–5145 (1967).
- Kim, J. S. *et al.* Warm-white-light emitting diode utilizing a single-phase full-color $\text{Ba}_3\text{MgSi}_2\text{O}_8$: Eu^{2+} , Mn^{2+} phosphor. *Appl. Phys. Lett.* **84**, 2931–2933 (2004).
- Daicho, H. *et al.* A novel phosphor for glareless white light-emitting diodes. *Nat. Commun.* **3**, 1132 (2012).
- Matsuzawa, T., Aoki, Y., Takeuchi, N. & Murayama, Y. New long phosphorescent phosphor with high brightness, SrAl_2O_4 : Eu^{2+} , Dy^{3+} . *J. Electrochem. Soc.* **143**, 2670–2673 (1996).
- Pan, Z., Lu, Y.-Y. & Liu, Y. Sunlight-activated long-persistent luminescence in the near-infrared from Cr^{3+} -doped zinc gallogermanates. *Nat. Mater.* **11**, 58–63 (2012).
- Nakamura, S., Mukai, T. & Senoh, M. Candela-class high-brightness InGaN-AlGaN double-heterostructure blue-light-emitting diodes. *Appl. Phys. Lett.* **64**, 1687–1689 (1994).
- Oto, T., Banal, R. G., Kataoka, K., Funato, M., Kawakami, Y. 100 mW deep-ultraviolet emission from aluminium-nitride-based quantum wells pumped by an electron beam. *Nat. Photon.* **4**, 767–771 (2010).
- Khan, A., Balakrishnan, K. & Katona, T. Ultraviolet light-emitting diodes based on group three nitrides. *Nat. Photon.* **2**, 77–84 (2008).
- Taniyasu, Y., Kasu, M. & Makimoto, T. An aluminium nitride light-emitting diode with a wavelength of 210 nanometres. *Nature* **441**, 325–328 (2006).
- Watanabe, K., Taniguchi, T., Niiyama, T., Miya, K. & Taniguchi, M. Far-ultraviolet plane-emission handheld device based on hexagonal boron nitride. *Nat. Photon.* **3**, 591–594 (2009).
- Lee, K. H. *et al.* Large-scale synthesis of high-quality hexagonal boron nitride nanosheets for large-area graphene electronics. *Nano Lett.* **12**, 714–718 (2012).
- McGehee, M. D. *et al.* Narrow bandwidth luminescence from blends with energy transfer from semiconducting conjugated polymers to europium complexes. *Adv. Mater.* **11**, 1349–1354 (1999).
- Garrido, B. *et al.* Excitable Er fraction and quenching phenomena in Er-doped SiO_2 layers containing Si nanoclusters. *Phys. Rev. B* **76**, 245308 (2007).
- Yu, M. *et al.* Fabrication, patterning, and optical properties of nanocrystalline YVO_4 :A ($\text{A} = \text{Eu}^{3+}$, Dy^{3+} , Sm^{3+} , Er^{3+}) phosphor films via sol-gel soft lithography. *Chem. Mater.* **14**, 2224–2231 (2002).
- Miniscaco, W. J. Erbium-doped glasses for fibers amplifiers at 1550 nm. *J. Lightwave Technol.* **9**, 234–250 (1991).
- Auzel, F. Upconversion and Anti-Stokes Processes with f and d Ions in Solids. *Chem. Rev.* **104**, 139–173 (2004).
- Layne, C. B., Lowdermilk, W. H. & Weber, M. J. Multiphonon relaxation of rare-earth ions in oxide glasses. *Phys. Rev. B* **16**, 10–20 (1977).
- Paulose, P. I., Jose, G., Thomas, V., Unnikrishnan, N. V. & Warriar, M. K. R. Sensitized fluorescence of $\text{Ce}^{3+}/\text{Mn}^{2+}$ system in phosphate glass. *J. Phys. Chem. Solids* **64**, 841–846 (2003).
- Caldino, U., Hernández-Pozos, J. L., Flores, C., Speghini, A. & Bettinelli, M. Photoluminescence of Ce^{3+} and Mn^{2+} in zinc metaphosphate glasses. *J. Phys.: Condens. Matter.* **17**, 7297–7305 (2005).
- Tanimizu, S. [Luminescence centers of ns^2 -type ions] *Phosphor Handbook 2nd Edition* [Yen, W. M., Shionoya, S. & Yamamoto, H. (ed)] [155–165], (CRC Press, Boca Raton, 2007).

21. Fukuda, A. Jahn-Teller effect on the structure of the emission produced by excitation in the A band of KI:Tl-type phosphors. Two kinds of minima on the $\Gamma_4^- (^3T_{1g})$ adiabatic potential-energy surface. *Phys. Rev. B* **1**, 4161–4178 (1970).
22. Ropp, R. C. & Mooney, R. W. Tin-Activated Alkaline-Earth Pyrophosphate Phosphors. *J. Electrochem. Soc.* **107**, 15–20 (1960).
23. Ehrt, D. Photoluminescence in the UV–VIS region of polyvalent ions in glasses. *J. Non-Cryst. Solids* **348**, 22–29 (2004).
24. Reisfeld, R., Boehm, L. & Barnett, B. Luminescence and nonradiative relaxation of Pb^{2+} , Sn^{2+} , Sb^{3+} , and Bi^{3+} in oxide glasses. *J. Solid State Chem.* **15**, 140–150 (1975).
25. Leskelä, M., Koskentalo, T. & Blasse, G. Luminescence Properties of Eu^{2+} , Sn^{2+} , and Pb^{2+} in SrB_6O_{10} and $Sr_{1-x}Mn_xB_6O_{10}$. *J. Solid State Chem.* **59**, 272–279 (1985).
26. Jimenez, J. A. *et al.* Silver aggregates and twofold-coordinated tin centers in phosphate glass: A photoluminescence study. *J. Lumin.* **129**, 1546–1554 (2009).
27. Butler, K. H. & Jerome, C. W. Calcium Halophosphate Phosphors I. Analysis of Emission Spectra. *J. Electrochem. Soc.* **97**, 265–270 (1950).
28. Masai, H., Takahashi, Y., Fujiwara, T., Matsumoto, S. & Yoko, T. High photoluminescent property of low-melting Sn-doped phosphate glass. *Appl. Phys. Express* **3**, 082102 (2010).
29. Masai, H. *et al.* Correlation between emission property and concentration of Sn^{2+} centre in the SnO - ZnO - P_2O_5 glass. *Opt. Express* **20**, 27319–27326 (2012).
30. Masai, H. *et al.* White light emission of Mn-doped SnO - ZnO - P_2O_5 glass containing no rare earth cation. *Opt. Lett.* **36**, 2868–2870 (2011).
31. Masai, H., Fujiwara, T., Matsumoto, S., Tokuda, Y. & Yoko, T. Emission property of Sn^{2+} -doped ZnO - P_2O_5 glass. *J. Non-Cryst. Solids* **383**, 184–187 (2014).
32. Masai, H. *et al.* Narrow energy gap between triplet and singlet excited states of Sn^{2+} in borate glass. *Sci. Rep.* **3**, 3541 (2013).
33. Masai, H., Miyata, H., Tanimoto, T., Tokuda, Y. & Yoko, T. Preparation of Sn-doped zinc phosphate amorphous thin film and its emission properties. *J. Am. Ceram. Soc.* **96**, 382–384 (2013).
34. Niida, H., Takahashi, M., Uchino, T. & Yoko, T. Preparation and structure of organic–inorganic hybrid precursors for new type low-melting glasses. *J. Non-Cryst. Solids* **306**, 292–299 (2002).
35. Morena, R. Phosphate glasses as alternatives to Pb-based sealing frits. *J. Non-Cryst. Solids* **263–264**, 382–387 (2000).
36. Masai, H. *et al.* Correlation between preparation conditions and the photoluminescence properties of Sn^{2+} centres in ZnO - P_2O_5 glasses. *J. Mater. Chem. C* **2**, 2137–2143 (2014).
37. Bekaert, E., Montagne, L., Delevoye, L., Palavit, G. & Wattiaux, A. NMR and Mössbauer characterization of tin(II)–tin(IV)–sodium phosphate glasses. *J. Non-Cryst. Solids* **345**, 70–74 (2004).
38. Geurts, J., Rau, S., Richter, W., Schmitte, F. J. SnO films and their oxidation to SnO_2 : Raman scattering, IR reflectivity and X-ray diffraction studies. *Thin Solid Films* **121**, 217–225 (1984).
39. Skuja, L. Isoelectronic series of twofold coordinated Si, Ge, and Sn atoms in glassy SiO_2 : a luminescence study. *J. Non-Cryst. Solids* **149**, 77–95 (1992).
40. D'Amico M., Messina, F., Cannas, M., Leone, M., & Boscaino, R. Homogeneous and inhomogeneous contributions to the luminescence linewidth of point defects in amorphous solids: Quantitative assessment based on time-resolved emission spectroscopy. *Phys. Rev. B* **78**, 014203 (2008).
41. D'Amico M., Messina, F., Cannas, M., Leone, M. & Boscaino, R. Photoluminescence spectral dispersion as a probe of structural inhomogeneity in silica. *J. Phys. Condens. Matter* **21**, 115803 (2009).
42. Muñoz F. A. & Rubio O. J. Fluorescence of tin-sensitized manganese in single-crystalline NaCl. *Phys. Rev. B* **38**, 9980–9986 (1988).
43. Reisfeld, R. & Lieblich-Soffer, N. Energy transfer from UO_2^{2+} to Sm^{3+} in phosphate glass. *J. Solid State Chem.* **28**, 391–395 (1979).
44. Aceves, R., Caldiño G. U., Rubio O. J. & Camarillo E. Nonradiative energy transfer $Sn^{2+} \rightarrow Mn^{2+}$ in monocrystalline KBr. *J. Lumin.* **65**, 113–119 (1995).
45. Masai, H. *et al.* Localized Sn^{2+} emission centre independent of the optical basicity of zinc phosphate glass. *Chem. Lett.* **42**, 132–134 (2013).

Acknowledgments

This work was partially supported by the Yazaki Memorial Foundation for Science and Technology, the Asahi Glass Foundation, the Research Institute for Production Development, a Collaborative Research Program of ICR Kyoto University (Grant #2013-62, #2014-31), the SPRITS program of Kyoto University, and a Grant-in-Aid for Young Scientists (A; Number 26709048). The work was also supported by ICR Grants for Young Scientists, and the Sumitomo Electric Industries Group CSR Foundation (to Y.Y. and Y.K.). The authors wish to thank Dr. Y. Tokuda (I.C.R., Kyoto Univ.) and Dr. K. Teramura (Kyoto Univ.) for their advice and discussion, and Dr. Y. Fujimoto (Kyushu Univ. Technol.) and Mr. Y. Hino (Kyoto Univ.) for their assistance with the QY measurements. The XAFS experiments were performed at the BL01B1 of SPring-8 with the approval of the Japan Synchrotron Radiation Research Institute (JASRI) (Proposal No. 2011B1193, 2014B1500). We also wish to thank Dr. T. Miyazaki (Tohoku Univ.) for the TEM and EDX-SEM measurements. The authors acknowledge Prof. T. Yoko passed away in 2014.

Author Contributions

H. Masai designed the research. H. Miyata and H. Masai executed the materials preparation and measurement except for the QY, luminescent dynamics, and XAFS measurements. H. Masai and S.O. performed the XAFS analysis. Y.Y. and Y.K. measured the luminescent dynamics. T.Y. and H. Masai measured the QY. H. Masai wrote the paper. All authors discussed the results.

Additional Information

Supplementary information accompanies this paper at <http://www.nature.com/srep>

Competing financial interests: The authors declare no competing financial interests.

How to cite this article: Masai, H. *et al.* Tin-Doped Inorganic Amorphous Films for Use as Transparent Monolithic Phosphors. *Sci. Rep.* **5**, 11224; doi: 10.1038/srep11224 (2015).



This work is licensed under a Creative Commons Attribution 4.0 International License. The images or other third party material in this article are included in the article's Creative Commons license, unless indicated otherwise in the credit line; if the material is not included under the Creative Commons license, users will need to obtain permission from the license holder to reproduce the material. To view a copy of this license, visit <http://creativecommons.org/licenses/by/4.0/>